

Single Image Reflection Removal with Physically-based Rendering

Soomin Kim
KAIST, Korea

soo.kim813@gmail.com

Yuchi Huo
KAIST, Korea

yuchihuo0000@gmail.com

Sung-Eui Yoon
KAIST, Korea

sungeui@kaist.edu

Abstract

Recently, deep learning based single image reflection separation methods have been exploited widely. To benefit the learning approach, a large number of training image-pairs (i.e., with and without reflections) were synthesized in various ways, yet they are away from a physically-based direction. In this paper, physically based rendering is used for faithfully synthesizing the required training images, and corresponding network structure is proposed. We utilize existing image data to estimate mesh, then physically simulate the depth-dependent light transportation between mesh, glass, and lens with path tracing. For guiding the separation better, we additionally consider a module of removing complicated ghosting and blurring glass-effects, which allows obtaining priori information before having the glass distortion. This module is easily accommodated within our approach, since that prior information can be physically generated by our rendering process. The proposed method considering the priori information as well as the existing posterior information is validated with various real reflection images, and is demonstrated to show visually pleasant and numerically better results compared to the state-of-the-art techniques.

1. Introduction

When taking a photo through a glass or a window, the foreground that is transmitted through the glass can be seen, but the reflection from the background is certainly captured as well. These reflections and dim transmission can be annoying for some cases or cannot be avoided, for example, when taking a photo of a skyscraper from an indoor room. As a result, removing the reflections from the input images can help us to generate better images and various computer vision techniques to work robustly and widely. Figure 1 shows one example case of capturing reflection when taking a picture inside a building toward the outside.

Physically, an image I with those reflections is a linear sum of the glass reflected background, \hat{R} , and the glass transmitted foreground, \hat{T} , as $I(x, y) = \hat{T}(x, y) + \hat{R}(x, y)$.

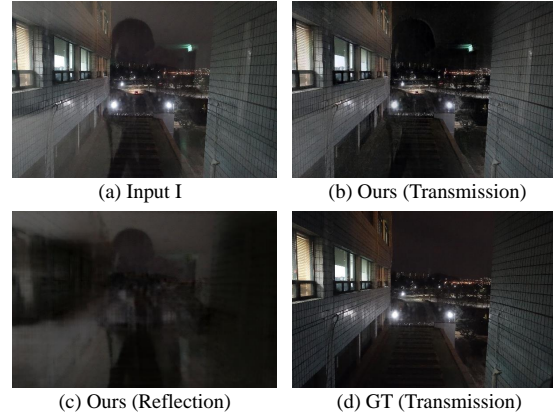


Figure 1: The result of our reflection removal method applied to a real-world image taken at night through a glass. Note that we can identify the reflection areas and remove most of them, while preserving the details of the transmission layer. GT indicates Ground Truth.

Since the number of unknown variables is twice the number of known in the equation, the problem is ill-posed, without using additional assumptions or priors.

Previous methods utilize multiple images of reflection with different conditions for obtaining some priors [1, 20, 13]. Especially, motion cue prior is widely used for separating the reflections from multi-images [7, 26, 8]. Although multiple-image reflection separation methods show reasonable results, it is not easy for users to capture constrained images as suggested in the prior approaches.

For single image reflection removal, natural image priors [15, 16, 17] or smoothness priors [18, 25] are used for formulating objective functions. Recent approaches [6, 29, 24, 27] started to utilize deep neural networks for removing the reflections on a single image. While training deep neural networks relies on a faithful dataset, most up-to-date methods synthesized datasets in an image space through a weighted addition between the foreground and the background, due to the difficulty of physically simulating the reflection and the transmission phenomena.

In this paper, we present a physically faithful training data generation method based on modeling and render-

ing techniques, such as depth estimation, geometry synthesizing and physically-based rendering. We utilize such physically-based rendered training images including the transmission and the reflection with and without posing a glass for training our deep learning architectures. Especially, we train glass-effect removal nets (*GR*-nets), which are used in reflection separation for better quality.

In summary, our contributions are as follows:

- Propose a synthesizing method to physically render a faithful reflection image dataset for training.
- Use *GR*-nets to transform the reflection image back to its prior-distortion status as a priori of the separation problem.
- Design a two-stages algorithm and dual loss terms to utilize both the (classical) posteriori and the (novel) priori information and achieve state-of-the-art results with real-world images.

2. Related Work

The reflection removal is a well known ill-posed problem and has been studied for a few decades. Since the problem itself is ill-posed, additional priors and assumptions are necessary for separating the reflection reasonably.

Single image-based methods with conventional priors. Since the single image methods lack information compared to the multi-image methods, they assume predefined priors. One of the widely used priors is the natural image gradient sparsity priors [16, 17]. These approaches decompose the layers with minimal gradients and local feature. Levin and Weiss [15] propose gradient sparsity priors with user labeling and show reasonable results. Another widely used assumption is that reflection layers are more likely to be blurred because of the different distance to the camera [18, 25]. In addition to that, Arvanitopoulos et al. [2] propose Laplacian fidelity term and l_0 gradient sparsity term to suppress reflections. Shih et al. [21] suggest to examine ghosting effects on the reflection and model them by GMM (Gaussian Mixture Models) patch prior.

Single image based methods with deep learning. Recent works start to adopt deep learning for the reflection removal problem. Fan et al. [6] propose a two-step deep architecture as the first network to estimate the edge of the reflection-free image, and reconstruct the image based on the estimated edge with the second network. Zhang et al. [29] adopt conditional GAN [10] with a combination of perceptual loss, adversarial loss and exclusion loss for separating reflection. Wan et al. [24] suggest a concurrent deep learning based framework for gradient inference and image inference. Yang et al. [27] propose a cascaded deep network for estimating both the background and the reflection.

Our method is also learning-based single image reflection removal method, but with two fundamental differentiations. First, we render physically faithful dataset to realistically reproduce lens focus and glass-effect. These visual effects vary depending on depth across the image space, but not faithfully captured by previous learning methods. Second, our method utilizes information not only after the images distorted by the glass, but also before the glass distortion, to get better separation and reconstruction results.

Synthesizing training datasets with rendering. Monte Carlo (MC) rendering is widely used in various applications for high-quality image synthesis. Its theoretical foundation includes the physical simulation of light transportation and the unbiased integration of incident radiances [28]. In order to simulate the shading effect of complex geometry details, displacement mapping is proposed to reconstruct geometry from a depth map [5]. Because physically-based rendering can faithfully simulate the physical process of light transportation, it has been proven a promising way to synthesize deep learning datasets for various computer vision problems. For example, Zhang et al. present a large 3D indoor scene dataset for scene understanding [30].

In this paper, we propose to use displacement mapping and path tracing to synthesize a physically plausible dataset for the reflection removal problem.

3. Overview

In this section, we briefly introduce the overall structure of our method. There are two main components in our reflection removal technique. The first part is synthetically generating training images with physically-based rendering, and the second part is network training using rendered training images.

To train the deep network, a large amount of reflection and reflection-free image pairs are necessary. However, it is quite troublesome to obtain many such kinds of image pairs. Most of the prior deep learning based reflection removal methods [6, 29, 24, 27] synthesized a reflection image by mixing two ordinary images, one as reflection and another as transmission, with different coefficients followed by applying Gaussian blurring on reflection and scaling down the brightness of transmission. The technical details vary from one to the other, but they synthesized the reflection images in an image space.

We found that instead of synthesizing the reflection images in the image space, rendering the reflection images in a three dimensional (3D) space would produce more realistic images for training, resulting in a higher removal accuracy. In order to achieve physically faithful dataset, we adopt a series of modeling and rendering techniques, i.e., depth estimation, geometry synthesizing and physically based rendering technique (path tracing [12]).

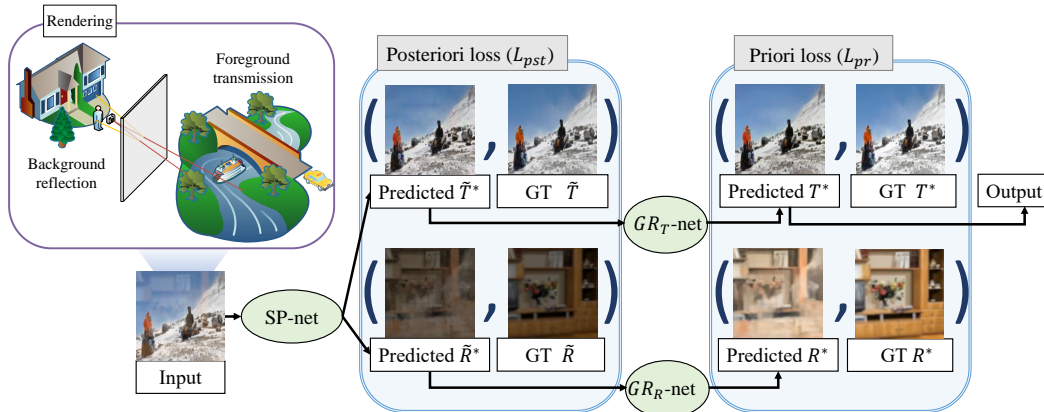


Figure 2: Overview of our algorithm. From a given image with reflection (I), our SP -net first separates I to predicted foreground transmission with glass-effect, \tilde{T}^* (since the scene is seen through the glass), and background reflection with glass-effect, \tilde{R}^* (background reflected by a glass). A loss is calculated with each of predicted value and its ground truth, and it is called posteriori loss (L_{pst}). Then our trained glass-effect removal networks, GR_T -net and GR_R -net, remove the glass effect of the predicted \tilde{T}^* and \tilde{R}^* into T^* and R^* , respectively. Since T^* and R^* are released from complicated glass-effects, we can better capture various image information, resulting in clearer error matching between the predicted images and their ground truths. So we calculate a new loss, priori loss (L_{pr}), between the priori images T^* and R^* and their GTs (Section 5.2). The entire separation network is trained with a loss combination of L_{pst} and L_{pr} .

Specifically, from 34 categories of the PLACES dataset [31], we randomly choose one image as a **foreground** transmission layer (*the side in front of the camera*) and another image as a **background** reflection layer (*the side behind the camera*). With one foreground and one background as a **scene** setup, we apply depth estimation [4] to extract the 3D model of the scene and then render it with path tracing to synthesize a group of images with or without reflection for training. Details of the method for synthesizing dataset are described in Section 4.

Figure 2 shows the overall pipeline of our network training algorithm using 5-image tuples as the training ground truth (GT). The algorithm contains a Separation network (SP -net), which separates the input image into two layers, and two Glass-effect Removal networks (GR -nets), which try to physically remove the glass-effect (e.g., blurring, attenuation, and ghosting) for better separation. As shown in Figure 3, we define foreground transmission image without any glass-effect as T , background reflection image without any glass-effect as R , transmission image seen through a glass as \tilde{T} , reflection image reflected by a glass as \tilde{R} , and the sum of \tilde{T} and \tilde{R} as I . Table 1 summarizes the notations that are used in the paper. The detailed explanation of each term is in Section 4.2. With these 5-image tuples, we first train the GR -nets, so that the \tilde{T} and \tilde{R} can be converted into T and R , then train the SP -net with all GT image tuples and the output of GR -nets.

Intuitively, the algorithm makes use of both the posteriori (with glass-effect) and the priori (without glass-effect) information. The posteriori information has been widely used by the existing methods. Specifically, those existing techniques try to directly separate an image distorted by the

Table 1: Symbols with * represent images predicted by the network; ones w/o * represent rendered or captured ground-truth (GT) images.

Symbol	Definition
T	Foreground image
R	Background image
\tilde{T}	Foreground image transmitted by a glass
\tilde{R}	Background image reflected by a glass
X^*	Predicted image X
T/R	T or R

glass-effect into a reflection and a transmission layer. To do that, various assumptions were introduced, such as the foreground is clear, but the background is blurred [6, 29, 27]. However, these assumptions do not always accord with various visual effects caused by the depth variation and lens (see Section 4 for more details). Furthermore, the complicated glass-effects hinder clear matching between predicted images and their ground-truth, resulting in a low-quality loss generation.

To address these issues, we found that the priori information can also provide important clues for the separation problem, in addition to the commonly used posteriori information. With the help of our GR -nets, we can physically predict the **inverse** process of adding glass-effect to an image. The output of GR -nets are actually prior-images, which reduce down various effects caused by the glass reflection and transmission. As a result, these prior-images without the glass-effect help clearer matching between predicted ones and their ground truth, improving the loss computation. Moreover, additional guide with these new priori

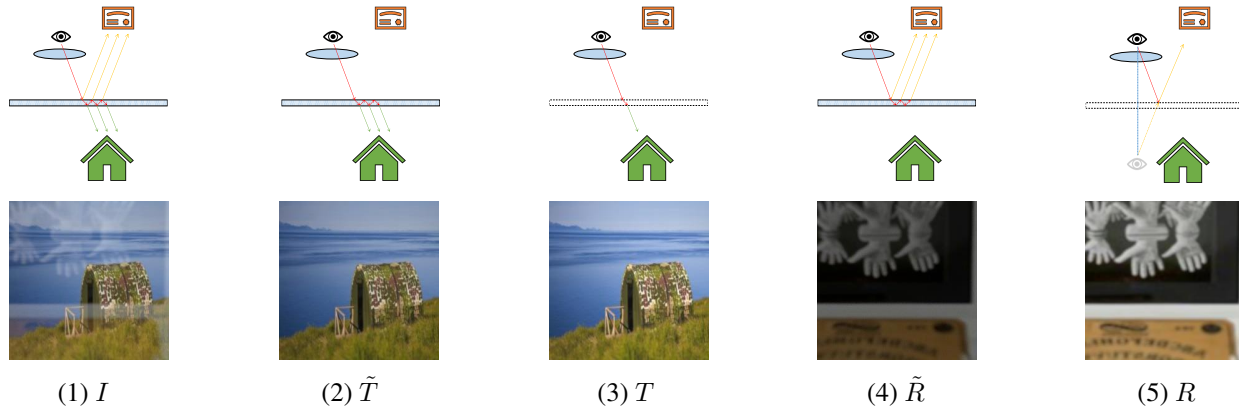


Figure 3: In this example, we set up a scene consisting of the foreground containing the house and background with indoor decorations. Suppose that we look at the foreground with a viewpoint behind a thin camera lens and a glass. (3) T contains foreground transmission only (T) without the glass effect. We simulate it with a **virtual glass**, which shifts the light path as a real glass, but does not cause any attenuation and distortion. (5) R is the background (reflection) image without any glass-effects. We obtain R reflected by the virtual glass for avoiding position shifting, similarly with T . (2) \tilde{T} and (4) \tilde{R} are computed by physically simulating the real-world attenuation and glass effect, i.e., multiple bounces within the glass. (1) I is the input image with reflection that sums (2) \tilde{T} and (4) \tilde{R} .

images helps on learning for the reflection removal problem and turning the transmission images back to the uncontaminated status.

4. Realistic Synthetic Dataset Generation

In order to achieve a physically faithful dataset, we adopt a series of modeling and rendering techniques, such as depth estimation, geometry synthesizing and physically based rendering. Our physically-synthesized dataset not only improves the network performance, but also provides a new perspective for fundamentally understanding and exploring the reflection removal problem on the physical ground.

4.1. Mesh Generation

In theory, the glass-effect and its physical light transmission effect are much more complex compared to the existing Gaussian blurring assumption adopted in prior techniques [6, 29, 27]. Simply speaking, a visible point is first reflected/refracted multiple times by the glass, resulting in ghosting or blurring. It is then defocused by the lens if it is outside the focus range. In other words, both objects in front and behind a glass are distorted, and the distortion effects are not uniform in the whole image, but depth-dependent.

For example, an object in the foreground (the side can be directly seen by the camera) might also show the blurring effect if it is outside the focus range, or ghosting effect if the gazing angle is small enough. Also, an object in the background (the side that can be seen by glass reflection) might not show any blurring effect if it is within the focus range. Figure 4 shows the change of our rendered dataset with various features.

Generating a variety of geometry meshes is the first block of physical simulation. Because modeling thousands of geometry scenes is economically prohibitive, we choose to utilize existing image dataset and depth information. Explored various RGBD dataset, but concerned about their limited environmental diversity, we choose the labeled RGB dataset for scene recognition [31] and adopt a depth estimation technique [4] to synthesize the depth channel. We selected 34 categories of the scenes (10 k images in total) from the dataset. Because the depth estimation method predicts only normalized relative depth, we manually scaled each category of the scene with an appropriated depth range; e.g., 2 m depth on average for the bedroom scene. Finally, the depth channel is fed into Blender [3] as a displacement map to export a geometry mesh from the input image. Figure 5 shows an example.

4.2. Rendering process

Given an RGB image and its corresponding mesh geometry, we attach the RGB channels of the image to the geometry surface to simulate the physical light transportation with a path tracing rendering technique [11]. For each scene, we randomly choose two images out of our image dataset as foreground and background, and render the scene by five different pipelines with a glass model in the middle. Figure 3 shows illustration of these five different images for a scenes. These five different rendered images include:

- I : An input image containing transmission plus reflection, where both foreground and background are rendered with the glass-effect, such as glass distortion, attenuation, and ghosting.
- \tilde{T} : foreground image transmitted by a glass with glass-



Figure 4: Images w/ and w/o depth and glass. (a) is a foreground w/o depth and glass; thus the whole image is sharp and clear. (b) is foreground w/ depth, but w/o glass, where the corners are blurred since they are outside the focus range; the focus is set to the center of the foreground, and thus its effect is subtle. (c) is foreground w/ depth and glass, where the color is attenuated and image are even more blurred due to the glass. (d) is background w/o glass and depth, so it is clean. (e) is background w/ depth, but w/o glass, where the whole image is blurred. (f) is background w/o depth and glass, where the glass further introduces attenuation, blurring and ghosting effect. (g) is the sum of (c) and (f).



Figure 5: A RGB image with the synthesized depth and mesh.

effect.

- T : The foreground image without any glass-effect. We simulate it with a **virtual glass** that warps the light path as a real glass, but does not cause any **ghosting and attenuation** effect. We use the virtual glass so that its pixels are pixel-wise consistent with those of \tilde{T} without any position shifting.
- \tilde{R} : The background image reflected by a glass with various glass-effects.
- R : The background reflection image without any glass-effect. We simulate it also with the **virtual glass** to calculate the reflective direction.

Note that all five images are rendered considering lens focusing with the estimated geometry, and thus blurring effect varies with object distances.

These 5-images decompose the whole glass reflection process into stand-alone steps and provide ample perspectives for extracting physical information for the reflection removal problem. Note that T and R are actually impossible to be captured by the real camera, since taking away a real-world glass will certainly make image points shifted and thus misaligned with I anymore. We explain how to use them within our network architectures in Sec. 5.

All images are rendered with a low-discrepancy sampler [11] with 512 sample per pixel, which is large enough to restrain visible noises. The glass is 20 millimeters of

thickness with random refractive index between 1.5 to 2.0, placed 50 centimeters in front of camera. We use 35 millimeter thin lens model with focus radius of 0.02. In order to simulate the real application scenario, we set the focus distance to the center of the foreground scene, so the foreground centers are always focused and the background reflection defocuses are depth-dependent. Overall, our synthetically generated dataset has 5000 image tuples for training and 100 image tuples for testing. Beside the synthesized dataset, we do not use any real-world images for training.

5. Proposed Network Architectures

In this section, we describe the proposed reflection removal algorithm based on the synthetically rendered dataset. We first discuss the overall architecture, followed by the loss functions for Glass-effect Removal nets (GR -nets) and Separation net (SP -net).

5.1. Network Architectures

Our model consists of three sub-networks. As illustrated in Figure 2, there are two separate glass-effect removal networks for background reflection effect (GR_R -net) and foreground transmission effect (GR_T -net), and a separation network (SP -net). Initially, the input image I is separated into \tilde{T}^* and \tilde{R}^* (Table 1) using the separation network (SP -net), and then they are fed into GR -nets for removing the glass-effect such as distortion, ghosting and attenuation. The final outputs of GR -nets are T^* and R^* , which are supposed to be devoid of glass-effect if the separation is perfectly carried.

In summary, the whole prediction model is as follows:

$$T^*/R^*(x, y) = GR_{T/R}(SP(I(x, y))). \quad (1)$$

For the sake of simplicity, we abuse the notation of / to indicate that T^* is computed by GR_T , and R^* is computed by GR_R . All of the three sub-networks SP -net, GR_T -net, and GR_R -net share the same structure, except that the SP -net has two outputs, but GR -nets have one output. They are

based on a conditional GAN adopted architecture proposed by Zhang et al. [29].

Layer Separation network, SP -net. As shown in Figure 2, the SP -net is designed to separate the input image I into transmission and reflection layers with glass-effect, i.e., \tilde{T}^* and \tilde{R}^* :

$$\tilde{T}^*, \tilde{R}^*(x, y) = SP(I(x, y)). \quad (2)$$

Note that the predicted \tilde{T}^* and \tilde{R}^* still contain various glass-effect.

Glass-effect Removal networks, GR -nets. The purpose of the GR -nets is to remove the glass-effect, such as distortion, ghosting, attenuation and blurring, from the output images of SP -net (\tilde{T}^* , \tilde{R}^*). Transmission glass-effect and reflection glass-effect are separately removed by GR_T -net and GR_R -net, respectively:

$$T^*/R^*(x, y) = GR_{T/R}(\tilde{T}^*/\tilde{R}^*(x, y)). \quad (3)$$

5.2. Loss function

Each individual sub-network has three loss terms: l_1 -loss, feature loss, and adversarial loss. l_1 -loss is widely used to measure the Euclidean distance between predicted one and its ground truth, and is also used for low-level information comparison for our method (we divide the sum of l_1 loss across the image by the total pixel number of the image). Our feature loss and adversarial loss are based on [29]. The feature loss L_{ft} is used for considering semantic information, and is calculated as a difference between features of the pre-trained VGG network Φ , when predicted and ground truth images are fed into Φ (Eq. 4). For obtaining realistic T images, the adversarial loss is adopted, as the many other recent works [29, 27, 14, 32]. A conditional GAN [10] model is utilized for this.

For explanation, assume that a function of a sub-network is f , its input is X , and its ground truth is Y . The feature loss L_{ft} is calculated as follows:

$$L_{ft}(f(X), Y) = \sum_l \gamma \|\Phi_l(Y) - \Phi_l(f(X))\|, \quad (4)$$

where Φ_l indicates the l -th layer of the VGG-19 network with the same layer selection of [29]; γ is the weighting parameter, which is empirically set to 0.2.

For the adversarial loss, the discriminator D of one sub-network is trained by:

$$\sum \log D(X, f(X)) - \log D(X, Y). \quad (5)$$

The adversarial loss is then defined as follows:

$$L_{adv}(X, f(X)) = \sum -\log D(X, f(X)). \quad (6)$$

Loss for SP -net. The purpose of the SP -net is separating \tilde{T}^* and \tilde{R}^* from the input I . Even though \tilde{T} and \tilde{R} are not our final targets, training the SP -net with the images with glass-effect can provide additional information for better separation; see Section 3. The first loss we calculate for training SP -net on its output (\tilde{T}^* , \tilde{R}^*) is *posteriori loss* (L_{pst} , with glass-effect). It is the combination of l_1 -loss, feature loss between \tilde{T}^*/\tilde{R}^* and \tilde{T}/\tilde{R} , and adversarial loss for \tilde{T}^* . After using GR -nets removing glass-effect of \tilde{T}^* and \tilde{R}^* , we also calculate the second loss term called *priori loss* (L_{pr}) between T^*/R^* and T/R . Since the SP -net does not need to create T^*/R^* directly, we do not use an additional adversarial loss for T^* :

$$L_{pst} = L_{l_1}(\tilde{T}^*, \tilde{T}) + L_{ft}(\tilde{T}^*, \tilde{T}) + L_{adv}(I, \tilde{T}^*) \\ + L_{l_1}(\tilde{R}^*, \tilde{R}) + L_{ft}(\tilde{R}^*, \tilde{R}), \quad (7a)$$

$$L_{pr} = L_{l_1}(T^*, T) + L_{ft}(T^*, T) \\ + L_{l_1}(R^*, R) + L_{ft}(R^*, R). \quad (7b)$$

Combining the above loss terms, our complete loss for SP -net is $L_{SP} = L_{pst} + L_{pr}$.

Loss for GR -net. The goal of both GR_T -net and GR_R -net is removing the glass effects from \tilde{T} and \tilde{R} , respectively. To train the networks, we formulate a combined loss function of l_1 -loss, feature loss and adversarial loss as follows:

$$L_{T/R} = L_{l_1}(T^*/R^*, T/R) + L_{ft}(T^*/R^*, T/R) \\ + L_{adv}(\tilde{T}/\tilde{R}, T^*/R^*). \quad (8)$$

Implementation. Each of our three sub-net shares the same structure based on the one proposed in [29], and they are fully convolutional networks with large 513×513 receptive fields for considering global information. Also, to evaluate separation quality in a semantic manner, VGG-19 [22] features pre-trained with the ImageNet dataset [19] are used as an hypercolumn features [9]. As Zhang et al. [29], we concatenate the input image with its hypercolumn features for the network input. For the training, we first train GR_T -net and GR_R -net with rendered image pairs independently, and then pre-trained GR_T -net and GR_R -net are connected to SP -net for SP -net training (GR -nets are fine-tuned in this stage). All of three sub-networks are trained by minimizing the aforementioned loss terms between ground truths and their predictions with a learning rate of 10^{-4} . The rendered training images have the 256×256 resolution.

6. Experiments with Real and Synthetic Data

We compare our approach with the state-of-the-art deep learning based reflection removal methods across different test sets that work for a given single image. We test on both real-world images and synthetic test dataset visually

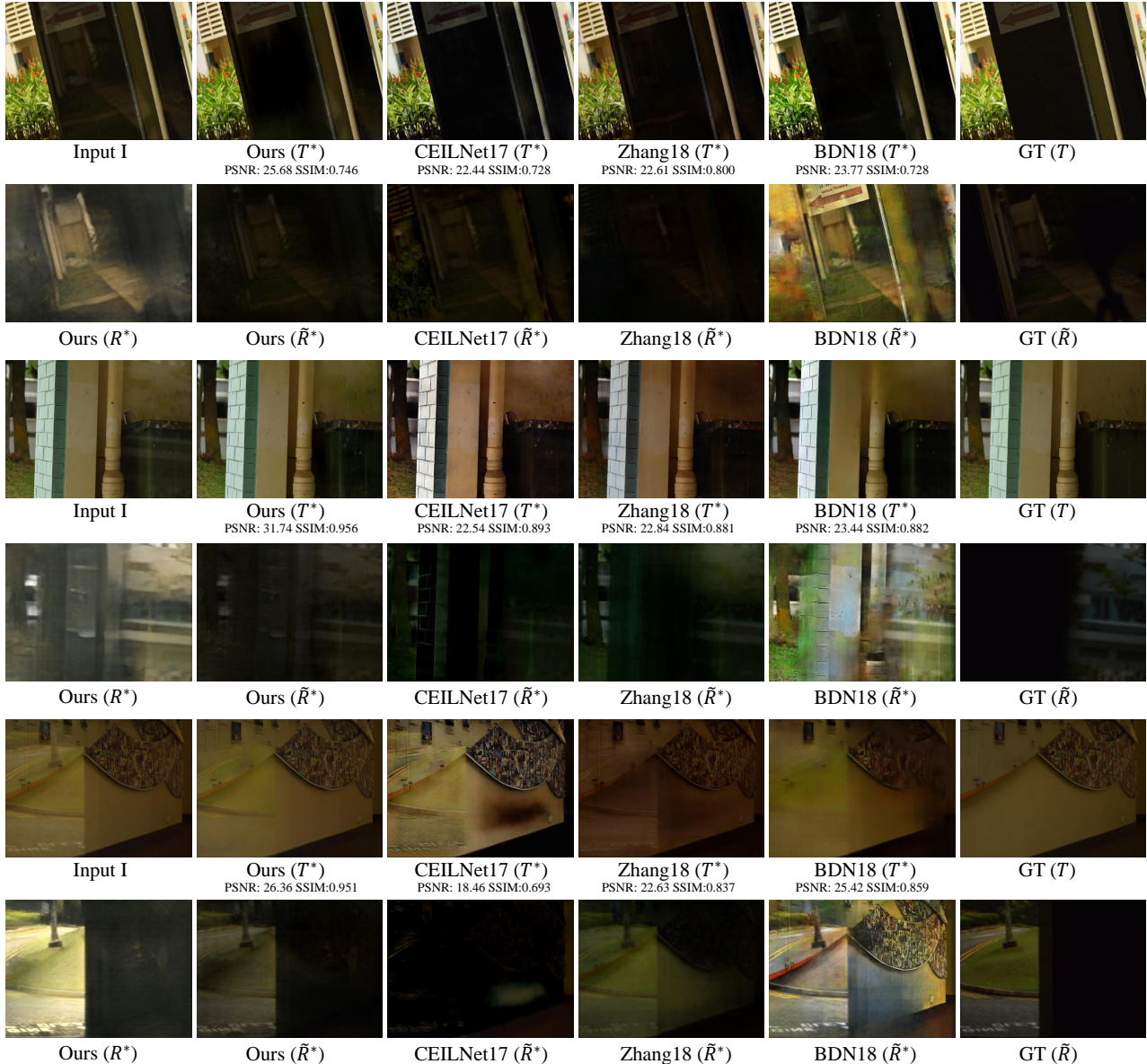


Figure 6: Examples of reflection removal result on three wild images, compared with CEILNet [6], Zhang et al. [29], and BDN [27]. Reported PSNR and SSIM are measured for each transmission image.

and quantitatively. For quantitative evaluation with real-world images, we utilize the well-known reflection removal benchmark, the SIR dataset [23]. It consists of three images (I, T, \tilde{R}) under various capturing settings from controlled indoor scenes to wild scenes. Since the indoor dataset is designed for exploring the impact of various parameters [23], we test our results on their wild scenes.

We also compare our results with those of CEILNet [6], Zhang et al. [29], and BDN [27]. We use pre-trained network weights provided from authors for obtaining all the results.

6.1. Quantitative evaluation

Table 2 shows quantitative results on the real-world test set and our rendered test set. The rendered test set includes 100 images synthesized by the method discussed in Section 4. We utilize SSIM and PSNR as error metrics, which are widely used in the prior reflection removal methods.

As the table shows, our method achieves clear numerical improvements in both real-world and rendered test sets on average. Improvement on the rendered test set is clearly expected, since our networks are trained with the rendered training dataset. Nonetheless, our approach shows

Method	SIR wild [23]		Rendered testset	
	PSNR	SSIM	PSNR	SSIM
Ours	23.43	0.875	27.37	0.935
CEILNet [6]	20.87	0.824	22.07	0.861
Zhang [29]	21.15	0.851	19.61	0.844
BDN [27]	22.00	0.835	22.13	0.842

Table 2: Quantitative results of different methods. Some result images of the SIR dataset can be found in Figure 6.



Figure 7: Qualitative comparison among ours, CEILNet [6], Zhang et al. [29], and BDN [27] on the CEILNet validation images.

an improvement even on the real-world dataset, thanks to our physically based rendering technique with the modeling process. Higher PSNR and SSIM mean closer to the ground-truth. The number on the table suggested that our method removes the reflection, while not degrading the transmission much compared to previous methods. Visual analysis with the SIR dataset is in the below section.

6.2. Qualitative evaluation

Figure 6 shows example results with the SIR wild test set; their corresponding quantitative analysis is in Table 2. The first case contains a lot of dark areas in the transmission layer that confuses most previous methods. CEILNet17 and BDN18 mistakenly treat the dark features as reflections, so over-remove them from the transmission layer, and Zhang18 identifies very little reflections. Yet our method can still work well with the dark transmission layer.

For the second case, some of the prior methods assume blurring objects to be from reflection, so they remove the de-focused tree and pipe in T^* . However, our method learned the depth-dependent, de-focus effects on the trans-

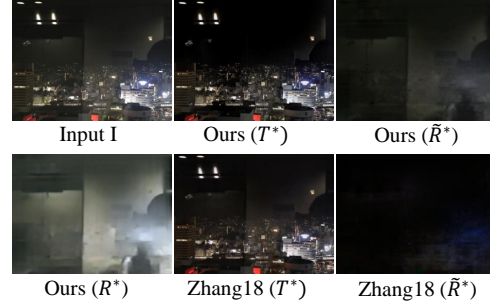


Figure 8: Challenging case. Strongly reflected light energy is hard to be removed since our dataset does not contain such type of data.

mission layer, thus does not remove much of the de-focused part in T^* and preserves the image color well.

For the last case, hard case, ours does not completely remove the reflection. Nonetheless, our \tilde{R}^* layer can identify and reasonably separate the location of the reflections, especially compared with the other tested methods.

We also evaluate different methods qualitatively on real-world images from CEILNet [6]. Note that this image set does not have ground truth \tilde{T} , and thus we do not report its quantitative result. Figure 7 shows example results on the CEILNet test set. Our method performs decently on the CEILNet dataset as well. Compared to the other methods, our GR_T -net removes most of the glass-effects without introducing significant sharpening, pixel position shifting or color mapping, while preserving natural image details and color tone.

7. Conclusion

We have proposed a novel learning-based single image reflection removal method, which utilizes reflection training images generated by physically based rendering. The training images consist of different types including transmission and reflection w/ and w/o the glass-effects and provide both classical posteriori and novel priori information. With the new dataset, we proposed SP -net to separate the input into two layers and GR -nets for removing the glass-effect in the separated layers. With the help of GR -net and the priori loss, the separation loss calculation is improved. We validated the effectiveness of our method with various real reflection images.

Limitation. While our method works well with a wide type of real images. It has a certain limitation. In an extreme case, there can be a strong reflection point if there is a light in the background (R) with relatively dark foreground (T). Since our training dataset does not contain those case, our method cannot recognize those parts as reflection and fails to remove it as shown in Figure 8.

References

- [1] A. Agrawal, R. Raskar, S. K. Nayar, and Y. Li. Removing photography artifacts using gradient projection and flash-exposure sampling. In *ACM Transactions on Graphics (TOG)*, volume 24, pages 828–835. ACM, 2005. 1
- [2] N. Arvanitopoulos, R. Achanta, and S. Susstrunk. Single image reflection suppression. In *Proceedings of the IEEE Conference on Computer Vision and Pattern Recognition*, pages 4498–4506, 2017. 2
- [3] Blender Online Community. *Blender - a 3D modelling and rendering package*. Blender Foundation, Blender Institute, Amsterdam, 2019. 4
- [4] W. Chen, Z. Fu, D. Yang, and J. Deng. Single-image depth perception in the wild. In *Advances in Neural Information Processing Systems*, pages 730–738, 2016. 3, 4
- [5] W. Donnelly. Per-pixel displacement mapping with distance functions. *GPU gems*, 2(22):3, 2005. 2
- [6] Q. Fan, J. Yang, G. Hua, B. Chen, and D. Wipf. A generic deep architecture for single image reflection removal and image smoothing. In *Proceedings of the IEEE International Conference on Computer Vision*, pages 3238–3247, 2017. 1, 2, 3, 4, 7, 8
- [7] K. Gai, Z. Shi, and C. Zhang. Blind separation of superimposed moving images using image statistics. *IEEE transactions on pattern analysis and machine intelligence*, 34(1):19–32, 2012. 1
- [8] B.-J. Han and J.-Y. Sim. Reflection removal using low-rank matrix completion. In *Proceedings of the IEEE Conference on Computer Vision and Pattern Recognition*, pages 5438–5446, 2017. 1
- [9] B. Hariharan, P. Arbeláez, R. Girshick, and J. Malik. Hypercolumns for object segmentation and fine-grained localization. In *Proceedings of the IEEE conference on computer vision and pattern recognition*, pages 447–456, 2015. 6
- [10] P. Isola, J.-Y. Zhu, T. Zhou, and A. A. Efros. Image-to-image translation with conditional adversarial networks. In *Proceedings of the IEEE conference on computer vision and pattern recognition*, pages 1125–1134, 2017. 2, 6
- [11] W. Jakob. Mitsuba renderer, 2010. <http://www.mitsuba-renderer.org>. 4, 5
- [12] J. T. Kajiya. The rendering equation. In *ACM SIGGRAPH computer graphics*, volume 20, pages 143–150. ACM, 1986. 2
- [13] N. Kong, Y.-W. Tai, and J. S. Shin. A physically-based approach to reflection separation: from physical modeling to constrained optimization. *IEEE transactions on pattern analysis and machine intelligence*, 36(2):209–221, 2014. 1
- [14] C. Ledig, L. Theis, F. Huszár, J. Caballero, A. Cunningham, A. Acosta, A. Aitken, A. Tejani, J. Totz, Z. Wang, et al. Photo-realistic single image super-resolution using a generative adversarial network. In *Proceedings of the IEEE conference on computer vision and pattern recognition*, pages 4681–4690, 2017. 6
- [15] A. Levin and Y. Weiss. User assisted separation of reflections from a single image using a sparsity prior. *IEEE Transactions on Pattern Analysis and Machine Intelligence*, 29(9):1647–1654, 2007. 1, 2
- [16] A. Levin, A. Zomet, and Y. Weiss. Learning to perceive transparency from the statistics of natural scenes. In *Advances in Neural Information Processing Systems*, pages 1271–1278, 2003. 1, 2
- [17] A. Levin, A. Zomet, and Y. Weiss. Separating reflections from a single image using local features. In *Proceedings of the 2004 IEEE Computer Society Conference on Computer Vision and Pattern Recognition, 2004. CVPR 2004.*, volume 1, pages I–I. IEEE, 2004. 1, 2
- [18] Y. Li and M. S. Brown. Single image layer separation using relative smoothness. In *Proceedings of the IEEE Conference on Computer Vision and Pattern Recognition*, pages 2752–2759, 2014. 1, 2
- [19] O. Russakovsky, J. Deng, H. Su, J. Krause, S. Satheesh, S. Ma, Z. Huang, A. Karpathy, A. Khosla, M. Bernstein, et al. Imagenet large scale visual recognition challenge. *International journal of computer vision*, 115(3):211–252, 2015. 6
- [20] Y. Y. Schechner, N. Kiryati, and R. Basri. Separation of transparent layers using focus. *International Journal of Computer Vision*, 39(1):25–39, 2000. 1
- [21] Y. Shih, D. Krishnan, F. Durand, and W. T. Freeman. Reflection removal using ghosting cues. In *Proceedings of the IEEE Conference on Computer Vision and Pattern Recognition*, pages 3193–3201, 2015. 2
- [22] K. Simonyan and A. Zisserman. Very deep convolutional networks for large-scale image recognition. In *ICLR*, 2015. 6
- [23] R. Wan, B. Shi, L.-Y. Duan, A.-H. Tan, and A. C. Kot. Benchmarking single-image reflection removal algorithms. In *Proceedings of the IEEE International Conference on Computer Vision*, pages 3922–3930, 2017. 7, 8
- [24] R. Wan, B. Shi, L.-Y. Duan, A.-H. Tan, and A. C. Kot. Crnn: multi-scale guided concurrent reflection removal network. In *Proceedings of the IEEE Conference on Computer Vision and Pattern Recognition*, pages 4777–4785, 2018. 1, 2
- [25] R. Wan, B. Shi, T. A. Hwee, and A. C. Kot. Depth of field guided reflection removal. In *2016 IEEE International Conference on Image Processing (ICIP)*, pages 21–25. IEEE, 2016. 1, 2
- [26] T. Xue, M. Rubinstein, C. Liu, and W. T. Freeman. A computational approach for obstruction-free photography. *ACM Transactions on Graphics (TOG)*, 34(4):79, 2015. 1
- [27] J. Yang, D. Gong, L. Liu, and Q. Shi. Seeing deeply and bidirectionally: A deep learning approach for single image reflection removal. In *Proceedings of the European Conference on Computer Vision (ECCV)*, pages 654–669, 2018. 1, 2, 3, 4, 6, 7, 8
- [28] S.-e. Yoon. *Rendering*. 2018. First edition. 2
- [29] X. Zhang, R. Ng, and Q. Chen. Single image reflection separation with perceptual losses. In *Proceedings of the IEEE Conference on Computer Vision and Pattern Recognition*, pages 4786–4794, 2018. 1, 2, 3, 4, 6, 7, 8
- [30] Y. Zhang, S. Song, E. Yumer, M. Savva, J.-Y. Lee, H. Jin, and T. Funkhouser. Physically-based rendering for indoor scene understanding using convolutional neural networks. In *Proceedings of the IEEE Conference on Computer Vision and Pattern Recognition*, pages 5287–5295, 2017. 2

- [31] B. Zhou, A. Lapedriza, A. Khosla, A. Oliva, and A. Torralba. Places: A 10 million image database for scene recognition. *IEEE Transactions on Pattern Analysis and Machine Intelligence*, 2017. 3, 4
- [32] J.-Y. Zhu, T. Park, P. Isola, and A. A. Efros. Unpaired image-to-image translation using cycle-consistent adversarial networks. In *Proceedings of the IEEE International Conference on Computer Vision*, pages 2223–2232, 2017. 6